Design of a Wire-Mesh Collimator for Gamma Cameras

M.-Iqbal Saripan, *Member, IEEE*, Maria Petrou*, *Senior Member, IEEE*, and Kevin Wells

***Abstract*—This paper presents a model of a wire-mesh collimator for a gamma camera that produces images of comparable quality as those produced with the conventional multihole collimator, but has about half the weight of the multihole collimator. The gamma camera and the collimator are simulated using the MCNPX code. Two final configurations of the wire-mesh collimator are proposed, and their performance is compared with other wire-mesh collimators and with the multihole collimator, using a point source, a planar square source, and two point sources, all in water. In all cases, photons with energy 140 keV are simulated. In addition, we use the simulation of a realistic phantom of a hot tumor in a warm background to assess the performance of our collimator in conjunction with an extended source.**

***Index Terms*—Gamma camera, multihole collimator, nuclear medicine, Wiener filtering, wire-mesh collimator.**

I. Introduction

THERE are many types of collimators used in conventional nuclear medicine, with the multihole collimator being the most commonly used one. The problem with this collimator is its weight. The multihole collimator is bulky, weighing more than 100 kg and, as a result, it is very difficult to handle. The aim of this paper is to propose the design of a lighter collimator, with comparable performance with that of the multihole collimator. This can reduce manufacturing costs and allow light-weight portable gamma cameras to be developed, something that will be particularly attractive in, for example, bedside cardiac imaging.

To address this problem the idea of a wire-mesh collimator was introduced recently by Chamberlain [7] and Ogawa and Kato [22], [23]. Such a collimator is made from a series of wire grids to reduce the collimator's weight. However, the performance of the wire-mesh collimators reported in the literature cannot match that of the multihole collimator. This paper proposes a design of the wire-mesh collimator that can successfully compete with the multihole collimator.

In the next section, we present the realistic model of the gamma camera that is used as a platform for image acquisition in this paper. This model is constructed using the Monte Carlo N-particles (MCNP) code, and its design is benchmarked against a Toshiba GCA 71000A clinical gamma camera. In some cases, we need image restoration to improve the quality of the captured images. So, Section III describes the image restoration method that we use in such cases, i.e., the Wiener filtering technique. In Section IV, we introduce the wire-mesh collimator, and present our algorithm for designing a viable configuration for it. Two new designs of a wire mesh collimator are proposed. In Section V, we choose parameters of the proposed collimators by investigating their performance in conjunction with a point source, a planar square source and two point sources. In Section VI, we test both proposed wire-mesh configurations with a more complex source. Finally, our conclusions are presented in Section VII.

II. Simulating a Realistic Camera and Imaging Environment

A. Monte Carlo N-Particle (MCNP) Code

The Monte Carlo technique is a numerical method for obtaining an estimate of the solution of a problem that depends on a random process, such as the distribution of photons emitted by a radioactive material and recorded by a gamma camera [30].

There are many types of the Monte Carlo simulation code available, such as MCNP [6], EGS4 [18], GATE [2], SIMSET [18], GEANT [4], SIMIND [10], and PETSIM [18]. In this paper, we simulate the gamma camera by using the MCNP code, version MCNPX.

Monte Carlo physics simulation packages attempt to provide essentially a "physics-library" of possible interactions. The user is required to specify the geometry of the system to be modeled, the source(s) to be used and the manner in which the resulting data are to be recorded. In the case of the MCNP Code, we define various geometric primitives, set up our source as a 140-keV gamma source and use one of the many tallies [6] to record the resulting data. We may specify the total number of events for the simulation to take place. During execution, the MCNP Code generates individual photons and tracks them through the user-defined geometry recording the various occurring interactions. Many such "photon histories" are then simulated in order to build up a statistically valid result, which may be in the form of an image or a deposited energy spectrum. In the experiments presented in this paper, we use tally F8 [6] in order to record the number of events in the gamma camera. In order to determine the exact location of the photon in the detector, we use another useful feature of the MCNP code, namely the particle track output card (PTRAC). PTRAC gives the location of every interaction which occurs in the detector and the energy deposited at that particular position.

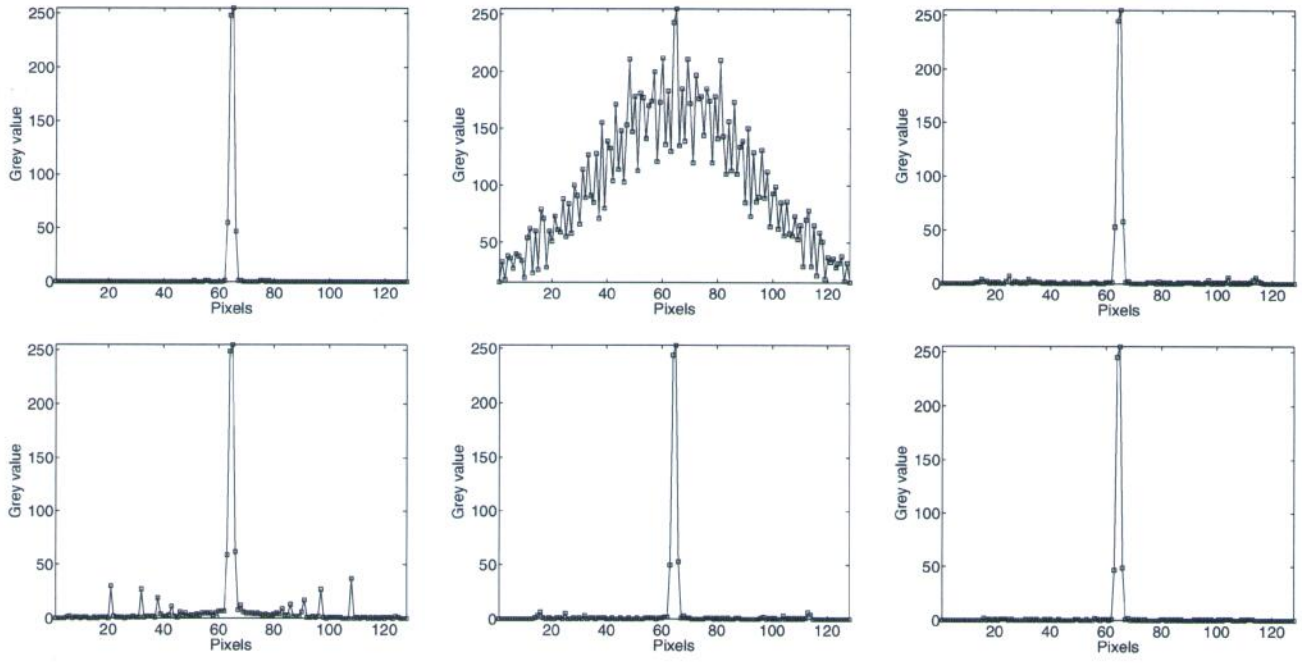

Fig. 6. Image cross sections for a point source for (top left) multihole collimator, (top middle) Chamberlain's, (top right) the first Ogawa and Kato's, (bottom left) the second Ogawa and Kato's, (bottom middle) the third Ogawa and Kato's, and (bottom right) the proposed configuration 18 of Table I.

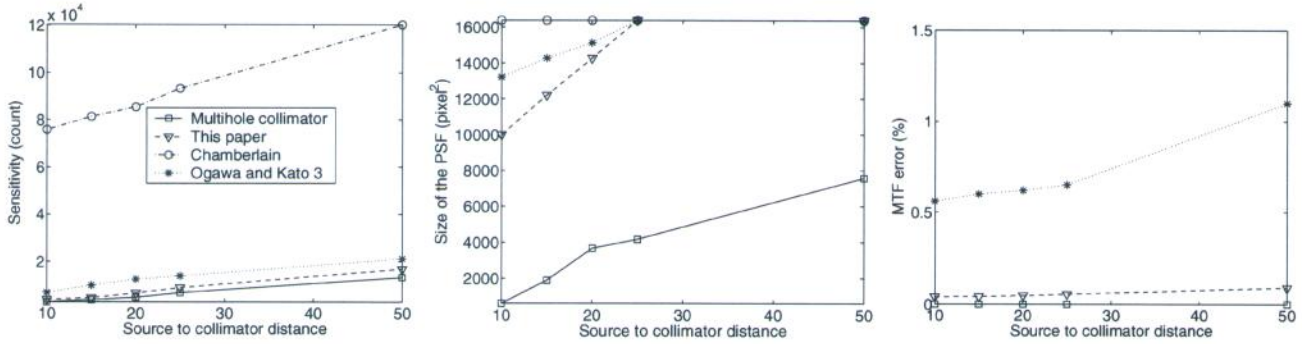

Fig. 7. (Left) Sensitivity, (middle) the size of the PSFs, and (right) the MSE of the MTFs for different locations of a point source in water. The MTF error for Chamberlain's structure was out of the scale of the graph.

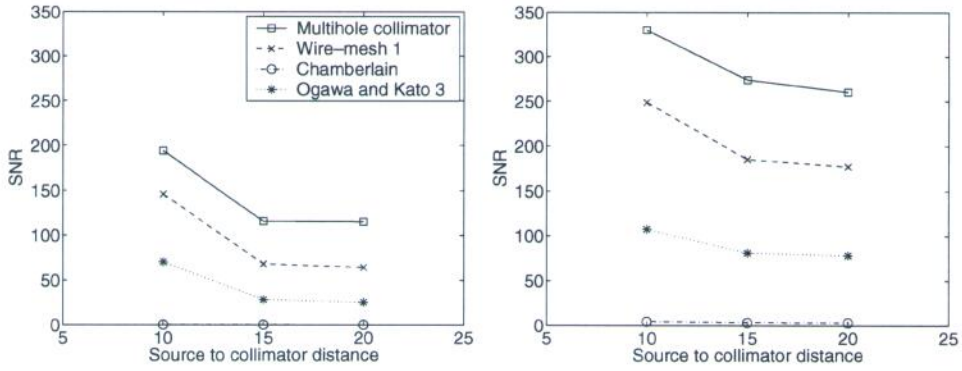

Fig. 8. SNR for different source to collimator distances for a planar square source (left) without and (right) with image postprocessing.

i.e., [2944–3054] (2999 ± 54.76). The size of its PSF is also very large, i.e., 100 × 100. However, the unwanted signal is very small, and that is reflected in the very small value of the MTF error.

In Fig. 7, we show the effect of the distance of the source from the collimator for the multihole collimator, Chamberlain's structure, the third structure given by Ogawa and Kato and our structure number 18.

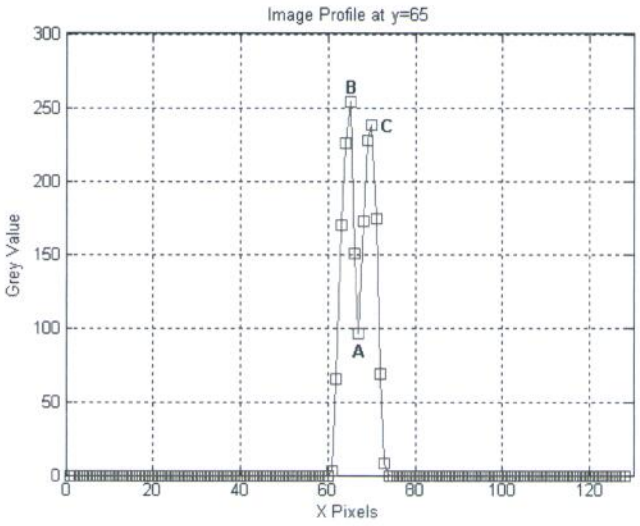

Fig. 9. Cross section of the image of two point sources. We accept that the two sources can be distinguished when the grey value at A is less than the grey values at B and C.

TABLE II
MINIMUM DISTANCE OF TWO POINT SOURCES IN ORDER TO CREATE DISTINCT PEAKS IN THE IMAGE (SEPARABILITY) OR TO BE PERCEIVED AS DISTINCT (RAYLEIGH CRITERION, RC)

Structure	Before restoration		After restoration	
	Separability (cm)	RC (cm)	Separability (cm)	RC (cm)
Multihole collimator	1.2	1.4	0.9	1.1
Wire-mesh WM-1, Nr 18	1.3	1.6	1.0	1.3
Chamberlain	2.2	2.6	2.0	2.4
Ogawa and Kato 3	1.3	1.6	1.0	1.3

TABLE III
RELAXING SOME DESIGN CONSTRAINTS

(d,c,a)	Weight loss (%)	Total number of photons	PSF size	MTF error (%)	SNR before	SNR after
(0.02, 0.15, 0.02)	60.5	3452	100 × 100	0.015	150.09	251.11
(0.03, 0.15, 0.02)	78.7	10591	128 × 128	1.309	34.21	110.96
(0.02, 0.20, 0.02)	73.3	11009	128 × 128	2.976	69.21	140.12
(0.02, 0.15, 0.01)	70.9	19543	128 × 128	2.387	10.92	76.31

The first panel of Fig. 7 shows the sensitivity,[3] measured by the number of detected photons. As we can see, the closest curve to the multihole collimator is given by our proposed structure, and the worst is given by Chamberlain's structure.

The middle panel of Fig. 7 shows the area of the PSF recorded by the detector. The PSF of Chamberlain's structure occupies the whole detector (the detector used was 128 × 128 pixels). The PSF of Ogawa and Kato's structure gets bigger and bigger,

[3]Under normal circumstances, high sensitivity is desirable. In this context, however, the word sensitivity refers to the number of detected photons. A number of detected photons above the range expected to be detected by the same camera using a multihole collimator and under the same imaging conditions, indicates that too many photons from undesirable directions are allowed to reach the detector.

TABLE IV
SENSITIVITY, THE SIZE OF THE PSFS AND THE ERROR OF THE MTF, OF VARIOUS CONFIGURATIONS OF THE NEW DESIGN OF THE WIRE-MESH COLLIMATOR

Experiment	Weight loss (%)	Total number of photons	PSF size	MTF error (%)
Add 2 mesh walls	59.7	3434	98 × 98	0.005
Add 4 mesh walls	58.9	3401	68 × 68	0.002
Add 6 mesh walls	58.2	3390	68 × 68	0.006
Add 8 mesh walls	57.4	3351	62 × 62	0.008
Add 10 mesh walls	56.6	3309	60 × 60	0.008
Add 12 mesh walls	55.8	3221	60 × 60	0.008
Add 14 mesh walls	55.1	3270	60 × 60	0.006
Add 16 mesh walls	54.3	3247	46 × 46	0.004
Add 18 mesh walls	53.5	3198	46 × 46	0.005
Add 20 mesh walls	52.7	3189	46 × 46	0.001
Add 22 mesh walls	51.9	3156	46 × 46	0.003
Add 24 mesh walls	51.2	3122	46 × 46	0.001
Add 26 mesh walls	50.4	3108	39 × 39	0.008
Add 28 mesh walls	49.6	3056	39 × 39	0.009
Add 30 mesh walls	48.8	3010	30 × 30	≈ 0
Add 32 mesh walls	48.0	2988	30 × 30	≈ 0

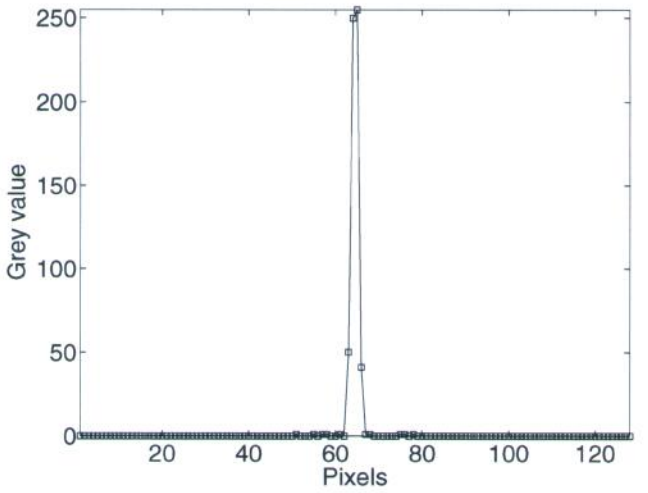

Fig. 10. Point source image produced from the configuration with 15 mesh entrance and 15 mesh exit walls.

and fills the whole detector as the source is placed further and further away from the collimator. Among all the presented configurations, the closest results to the multihole collimator are given by our structure. However, even this structure for some distances has a PSF that occupies the whole detector.

Finally, we also observe that the difference between the MTF of the multihole collimator, and the MTFs of the other structures, places our structure in the best position (last panel of Fig. 7). However, the sensitivity of the proposed structure is too high for it to be a replacement of the multihole collimator. There are two ways to improve it: using image post processing or redesigning it by introducing walls at both ends. Before we discuss

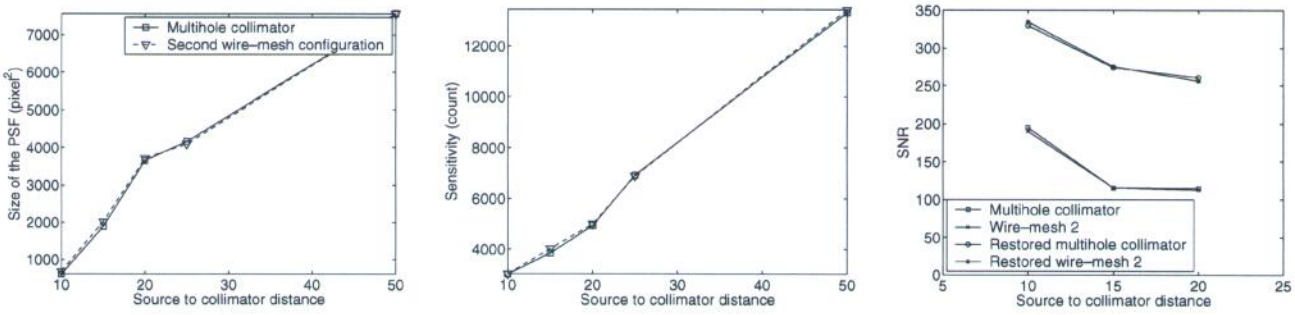

Fig. 11. (Left) Size of the PSF, (middle) sensitivity, and (right) SNR of the planar square source of our second wire-mesh configuration and the multihole collimator.

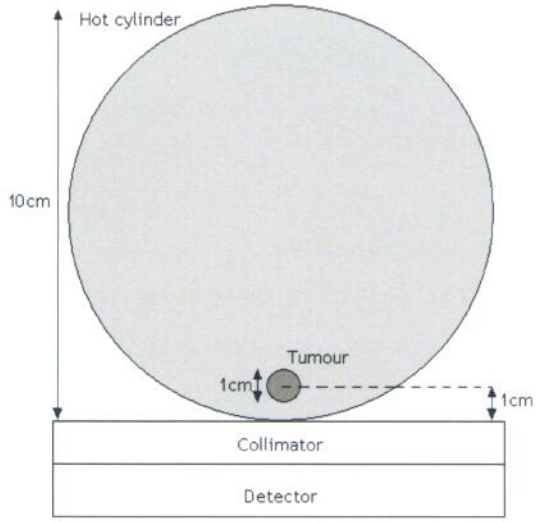

Fig. 12. Cross section of the experimental set-up of experiments A and B. The tumor is located 1 cm above the collimator and inside the water cylinder.

these options, we shall consider the quality of images produced in terms of image fidelity, by using a square planar source, and in terms of discriminating ability, by using two close-by point sources.

2) Planar Square Source: In this experiment, we simulate a planar square source of size 4 cm × 4 cm, located in water 10 cm above the collimator. The number of photons used is 10^9. We use the point spread function for each configuration, as worked out in the previous section, and Wiener filtering to improve the captured images. Using the SNR as a measure of image quality, the best configuration is the one for which the restored image has comparable quality as the raw image of the multihole collimator. The SNR is defined as the ratio between the average grey value inside the known extent of the source and the average grey value outside the source.

The results are shown in the last two columns of Table I. We can see that even the *postprocessed* images produced by Chamberlain's [7] and Ogawa and Kato's [22], [23] configurations cannot match the quality of the *raw* image of the multihole collimator. The first of our configurations that can produce a better restored image than the raw image of the multihole collimator is configuration 16, but the best quality of restored image is given by configuration 17. However, taking the factor of weight reduction into account, structure 18 is the best.

The effect of the distance of the source to the quality of the produced image is shown in Fig. 8.

3) Two Point Sources: The next step is to investigate the resolution limit of these configurations. We use two criteria for this. The first criterion is the source separability. The separability of two point sources may be determined by examining a cross-section of the created image. Based on Fig. 9, the two point sources are considered to be resolvable when the two peaks B and C have greater intensity than A.

The second criterion is the Rayleigh criterion [14]. This criterion is used in optics to describe the resolution limit of the human eye. The Rayleigh criterion states that two equally bright points or parallel lines can just be resolved from their image when the central maximum of the image of one of the sources coincides with the first minimum of the image of the second of the sources.

The results are shown in Table II. The entries in this table are the minimum distances of the two point sources for which either the brightness at point A was smaller than the brightness at points B and C, as defined in Fig. 9, or the Rayleigh criterion for the separability of the two point sources was fulfilled. From these results, we can see that the proposed structure 18 and the third Ogawa and Kato's structure perform identically. In all images, the locality shift is zero, i.e., all recorded peaks were at their expected locations.

4) Testing the Optimality of the Proposed Structure: We arrived at the final dimensions of the proposed structure in an algorithmic way, which, for example, meant that the intermesh distance had always to be the same as the wire radius. In this section we investigate whether the structure we arrived at could be improved by relaxing the restrictions of our algorithmic approach. So, we examine the performance of a mesh collimator with wire radius, a, 0.01 cm, instead of 0.02 cm, intermesh distance, d, 0.03 cm, instead of 0.02 cm, or intersepta space, c, 0.16 cm, instead of 0.15 cm. The performance of these changed configurations in comparison with configuration 18 of Table I is shown in Table III. These results show that although the way we reached our first design was somewhat restrictive, its performance is best among some other configurations that could be designed by relaxing the restrictions of our algorithmic approach.

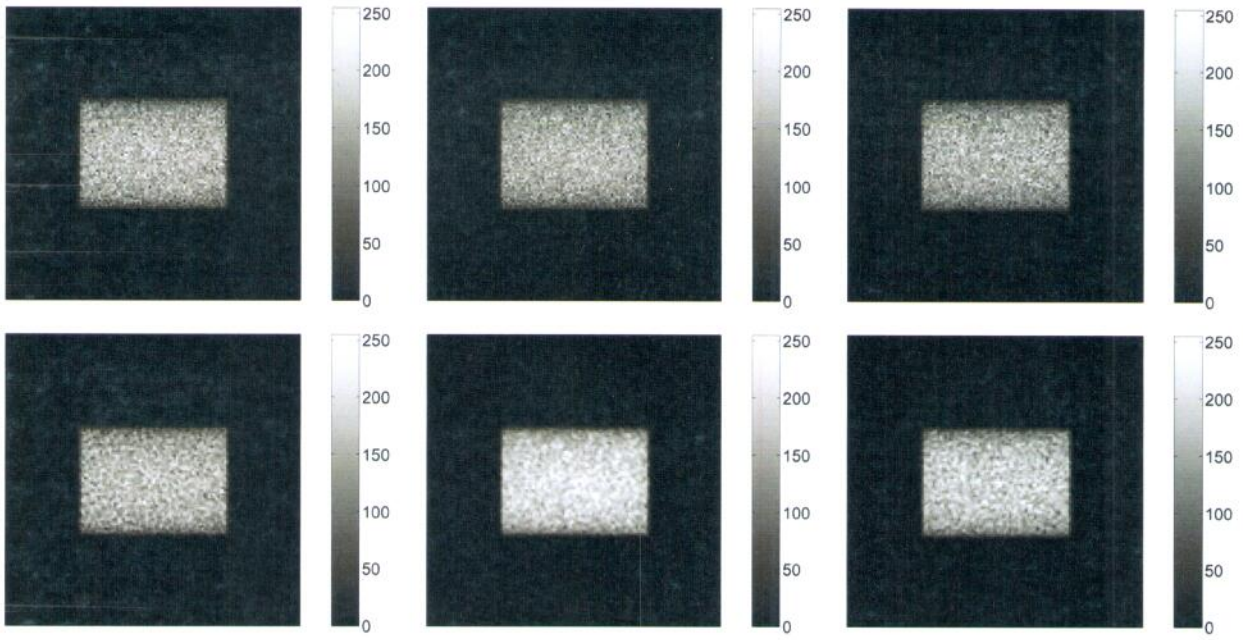

Fig. 13. Images of the phantom with TBR 2:1 from the multihole collimator, the first proposed wire-mesh collimator and the second proposed wire-mesh collimator from left to right, respectively, (top) without and (bottom) with Wiener filtering post processing. The tumor, a bright spot in the middle, is not actually discernible.

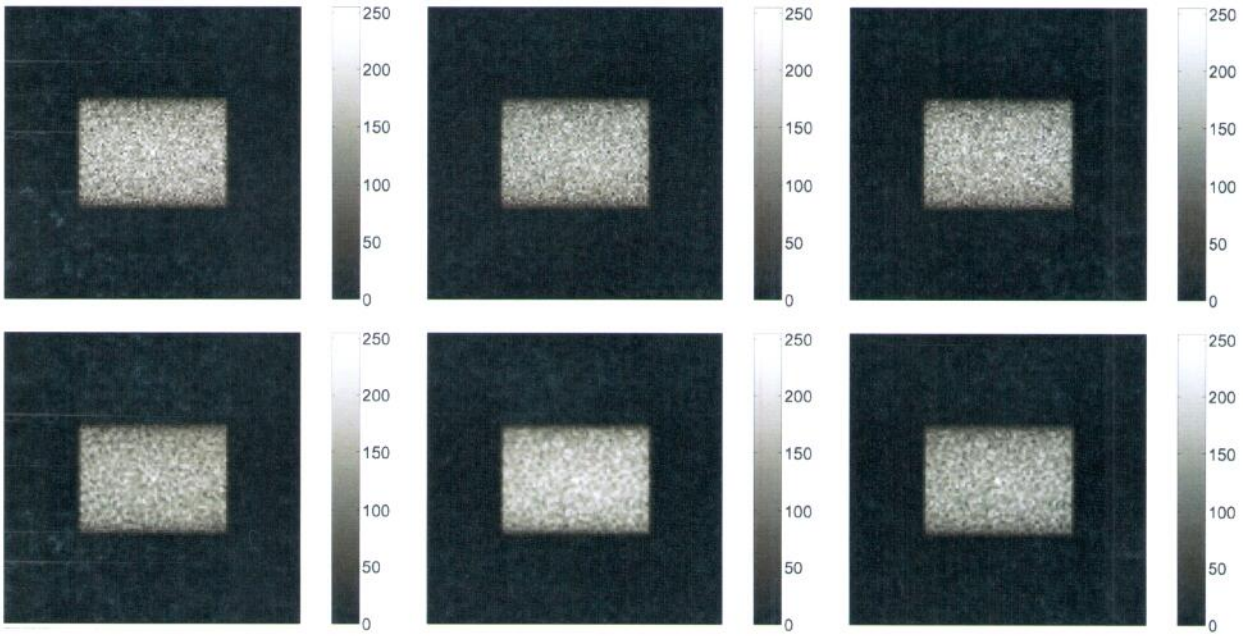

Fig. 14. Images of the phantom with TBR 3:1 from the multihole collimator, the first proposed wire-mesh collimator and the second proposed wire-mesh collimator from left to right, respectively, (top) without and (bottom) with Wiener filtering post processing. The tumor in the middle is just discernible.

B. Assessing the Performance of WM-2

The performance of the second collimator design we propose, when imaging an ideal point source, is shown in Table IV. In terms of sensitivity, the number of photons detected by the configurations with 14 or more meshes forming the walls is within the acceptable range of the statistical counting fluctuations, i.e., [2944–3054] (2999 ± 54.76). However, we can see that in terms of size of the PSF, only configurations with at least 30 or 32 mesh walls have the same size PSFs as the multihole collimator. The difference of the MTFs of these configurations from the MTF of the multihole collimator is negligible. Since we are interested in the lightest structure, the configuration with 30 meshes forming the walls is picked as the second configuration proposed in this paper.

This configuration can match the performance of the multihole collimator and has a weight reduced by 48.8%. The profile of the point source image of this configuration is shown in

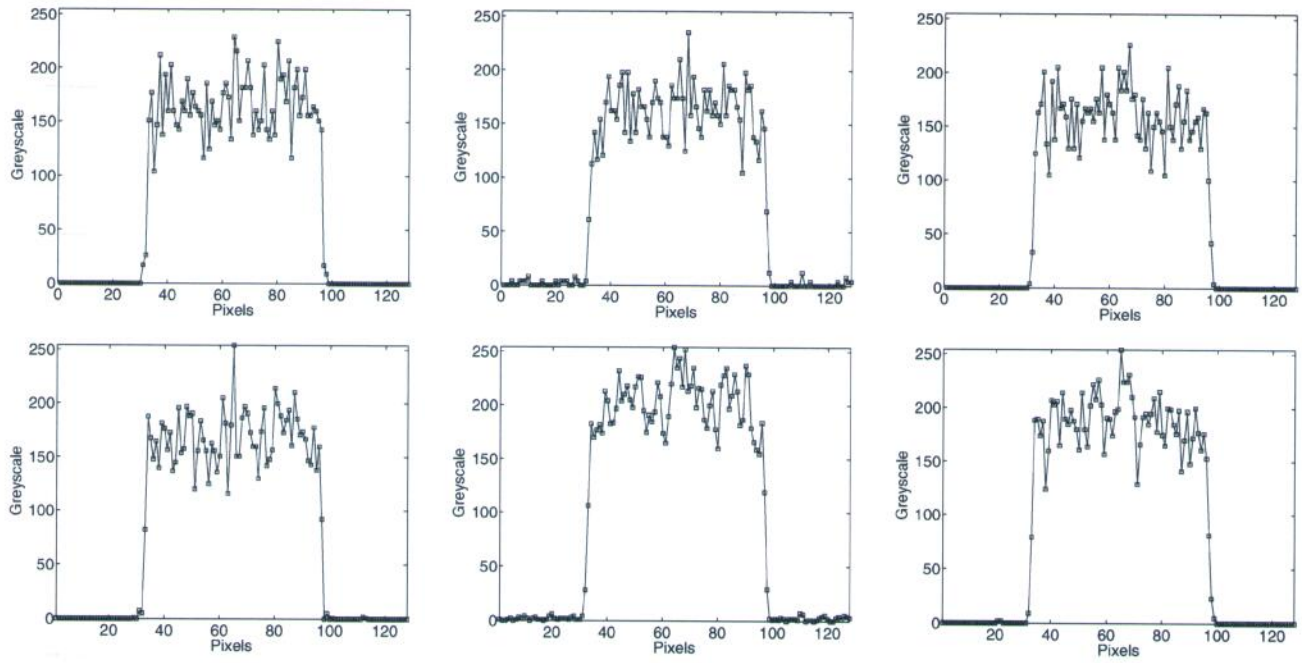

Fig. 15. Cross-sectional profiles of the images of Fig. 13.

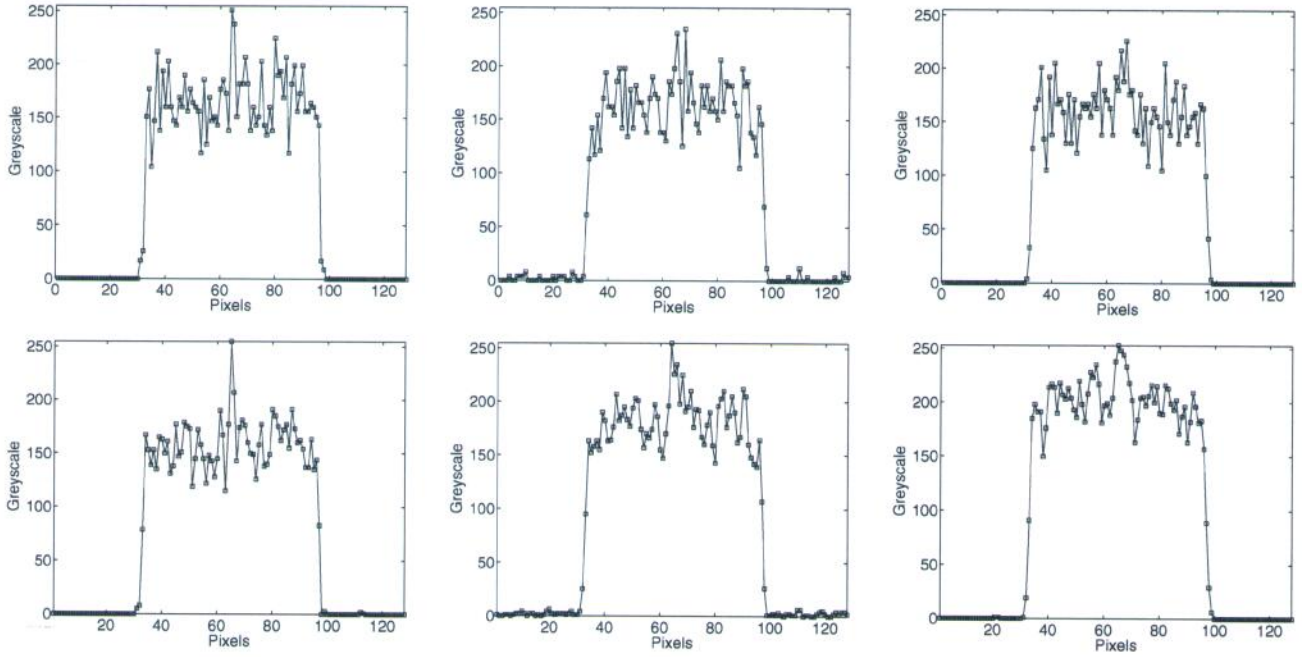

Fig. 16. Cross-sectional profiles of the images of Fig. 14.

Fig. 10. Comparing this image with that of the optimal configuration proposed by Ogawa and Kato [22], [23], we can see that this configuration does not produce any secondary peaks.

This new configuration with the 30 mesh walls produces an image with SNR = 192.12 before image postprocessing and SNR = 331.87 after Wiener filtering, when used for imaging a planar square source in water. The dependence of this performance on the distance from the source is shown in the far right graph of Fig. 11.

In conjunction with two point sources, this configuration yields a resolution distance of 1.0 and 1.2 cm in air and water, respectively. With Wiener filtering, the resolution is increased to 0.7 and 0.9 cm in air and water, respectively. For the Rayleigh criterion, the values are 1.3 and 1.4 cm in air and water, respectively. Wiener filtering improves the resolution to 0.8 and 1.1 cm in air and water, respectively.

These results show that our second structure has similar characteristics as the multihole collimator. Therefore, it offers a di-

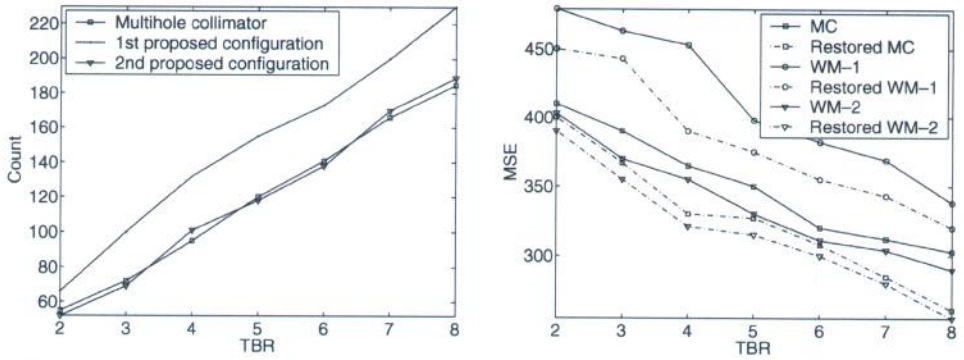

Fig. 17. Experiment A: The number of photons detected solely from (left) tumor and (right) the MSE. Abbreviation MC is for the multihole collimator, WM-1 is for the first optimal configuration of the wire-mesh collimator, and WM-2 is for the second optimal configuration of the wire-mesh collimator.

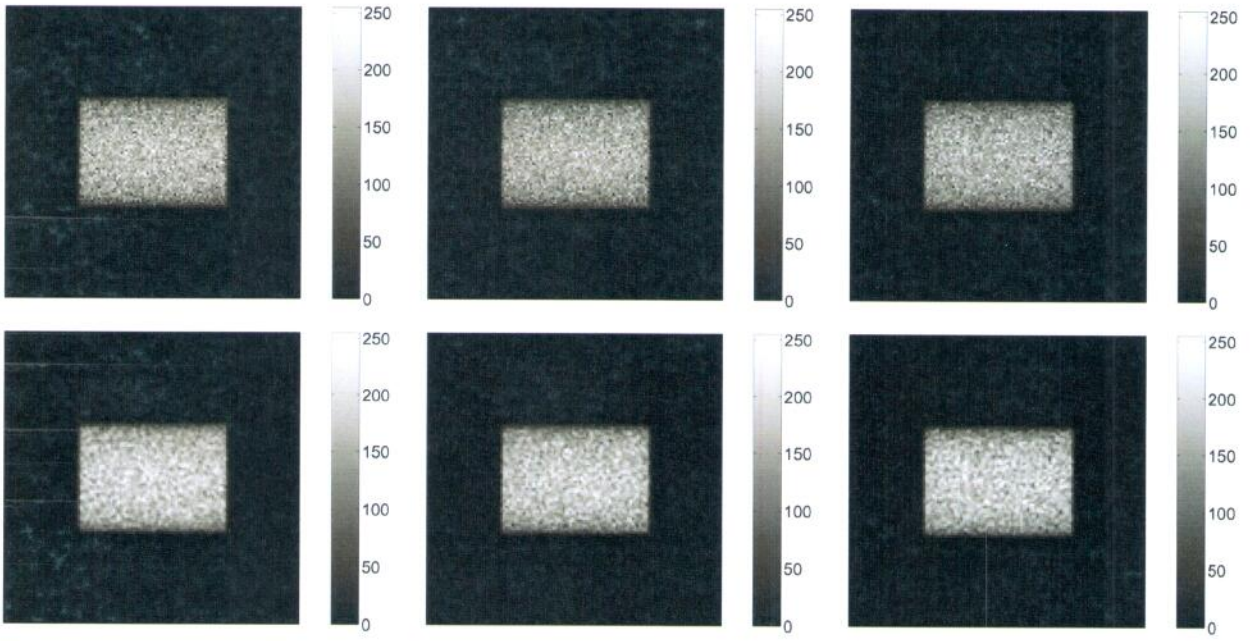

Fig. 18. Images produced for TBR 10:1 from a tumor of size 0.6 cm from the multihole collimator, the first wire-mesh collimator and the second wire-mesh collimator, from left to right, respectively, (top) without and (bottom) with Wiener filtering. The tumor in the middle is not really discernible.

rect replacement for the multihole collimator, without even the need of image post processing.

VI. Simulated Phantom Experiments

In this section, we use the two wire-mesh collimators we propose as well as the reference multihole collimator and test all three configurations with simulations of a realistic phantom.

We use a hot water cylinder[4] to provide the background radiation of the system. To decrease the running time of the MCNPX code, we place the cylinder directly on top of the collimator.

To model the tumor itself, we use a spherical lesion filled with soft tissues, with various tumor-to-background ratios (TBR) [13], [19], [26]. The TBR indicates the tumor level of activity. For example, a 5:1 tumor is half as active as a 10:1 tumor. In this paper, the background radiation is fixed to 2×10^9 photons, and based on this, we may calculate the number of photons that are projected by the tumor, depending on its TBR. The TBR is calculated based on the ratio of the source concentration, as [26]

$$\mathrm{TBR} = \frac{A_s}{A_b} \tag{3}$$

where A_s is the number of photons from the tumor per cm^3 and A_b is the number of photons from the background per cm^3.

There are two factors that influence the quality of the produced image, and which we wish to investigate in this paper: the TBR and the size of the lesion. For the first set of experiments (experiment A), we fixed the size of the lesion to 1 cm in diameter, and we simulated the 2:1–8:1. TBR cases. For the second experiment (experiment B), we fixed the TBR to 10:1, and observed the results for 0.5 cm–8 cm lesion diameters. For all the experiments, the location of the lesion was 1 cm away from the collimator and inside the cylinder. The experimental set-up is shown in Fig. 12. The image quality measure we use

[4]The water cylinder is filled with uniformly distributed sources of 140-keV photons.

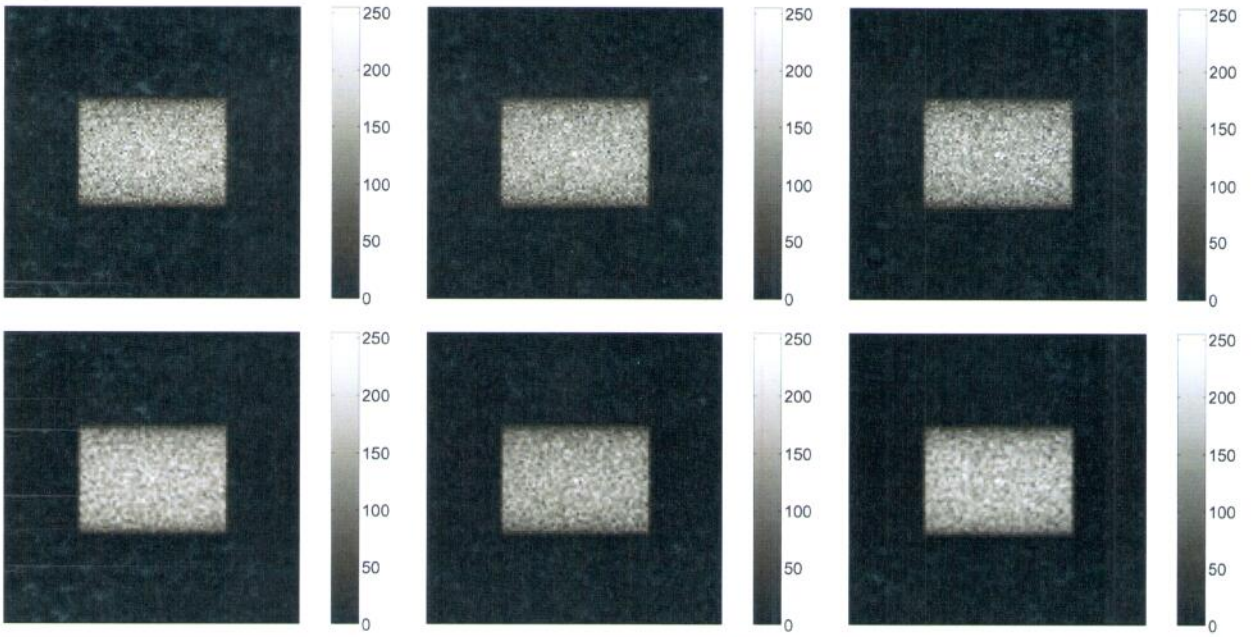

Fig. 19. Images produced for TBR 10:1 from a tumor of size 0.7 cm from the multihole collimator, the first wire-mesh collimator and the second wire-mesh collimator, from left to right, respectively, (top) without and (bottom) with Wiener filtering. The tumor in the middle is just discernible.

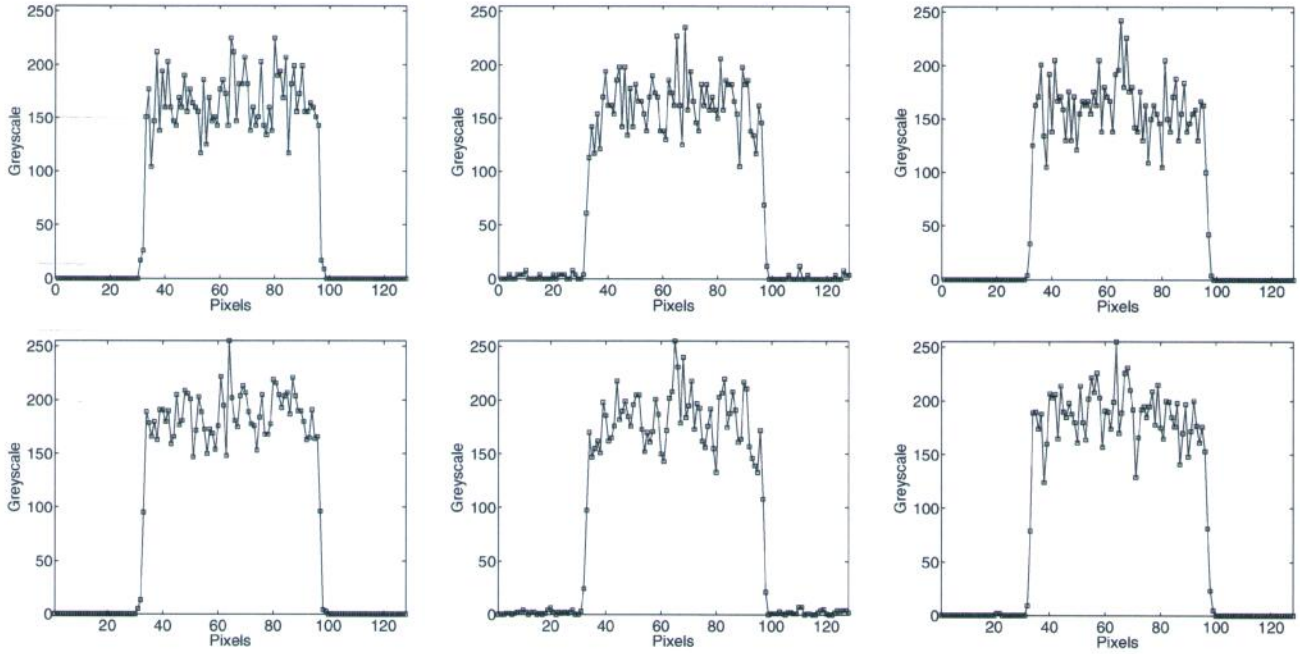

Fig. 20. Cross-sectional profiles of the images in Fig. 18.

is the MSE, because it can handle the fluctuations of the background radiation.

A. *Results and Discussion*

The experiments in this section are done in two steps: one simulation with a hot cylinder and a cold lesion for the background radiation, and another simulation with a hot lesion and a cold cylinder for the tumor. To model the complete source, the number of detected photons in the first step is added to the number of detected photons in the second step. The background radiation is simulated only once for each configuration, using 2×10^9 photons, but the number of photons from the tumor varies, depending on the TBR and the size of the lesion.

There are three structures that we used to capture the photons: the multihole collimator, the proposed wire-mesh collimator WM-1 Nr 18 and the second proposed wire-mesh collimator WM-2, with the 30 mesh walls.

1) Dependence of the Detection on the TBRs: The images we show in Figs. 13 and 14 correspond to the TBRs of the cases near

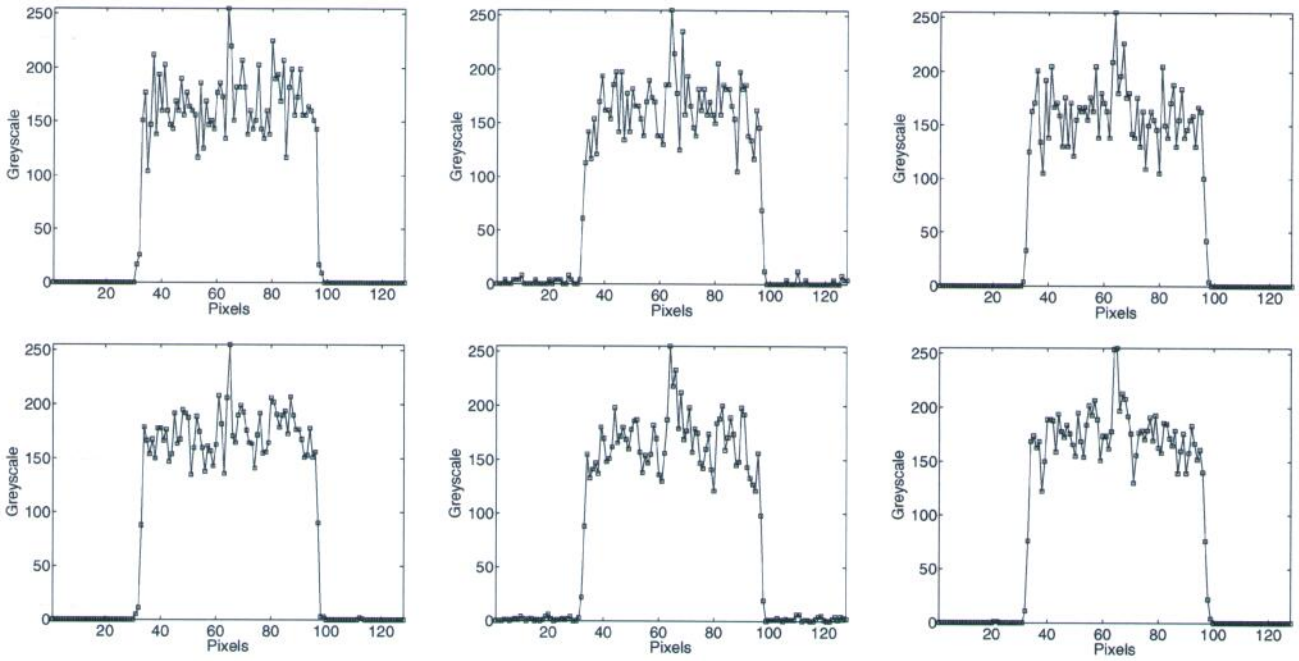

Fig. 21. Cross-sectional profiles of the images in Fig. 19.

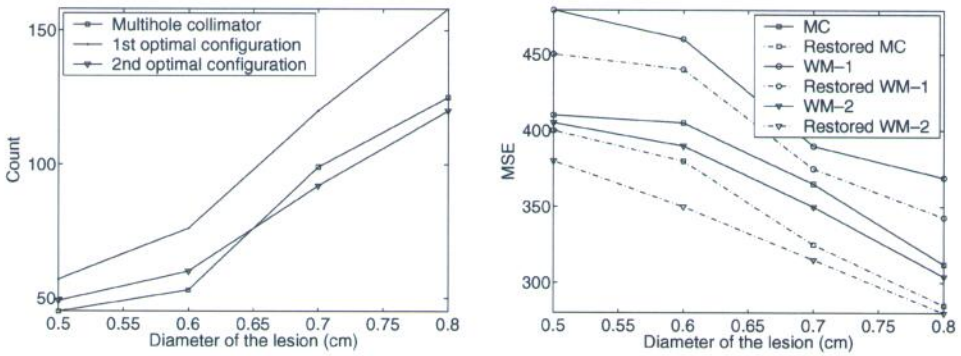

Fig. 22. Experiment B: The number of photons detected solely from the (left) tumor and (right) the MSE.

the discriminability threshold, i.e., TBR 2:1 and 3:1, respectively. The corresponding image profiles are shown in Figs. 15 and 16, respectively.

For the multihole collimator, we can see that the tumor starts to be visible in the restored image of the 3:1 TBR case. Without using Wiener filtering, the tumor can only be seen for the cases of TBR 4:1 and above. For the cases of TBR 2:1 and 3:1, we can see that the main peak that corresponds to a tumor does not reach the maximum value of 255 grey level in the images produced by the first wire-mesh collimator. This indicates that there is another pixel in these images that has more brightness than the tumor itself, and this could lead to a false diagnosis. With Wiener filtering, the brightness of the main peak is increased and the false peaks are suppressed.

Fig. 17 shows the quantitative version of our observations. We can see that the multihole collimator and the second wire-mesh collimator detected almost the same number of photons, because this wire-mesh collimator was designed exactly to match the performance of the multihole collimator. Although in terms of MSE values the second wire-mesh collimator we propose appears to be better than the reference multihole collimator, we consider this to be fortuitous. We believe that the reason of this difference is the random nature of these experiments. The reason this better performance appears to persist for all values of TBR, is because we used the same background radiation for all cases. That is, only the tumor was re-simulated as the TBR changed.

2) Dependence of the Detection on the Size of the Lesion: The images presented in Figs. 18 and 19 are the images produced from the multihole collimator, the first proposed wire-mesh collimator and the second proposed wire-mesh collimator, respectively, for the cases of fixed TBR to 10:1 and lesion sizes 0.6 and 0.7 cm, respectively. The cross sections of these images are shown in Figs. 20 and 21, respectively. In all cases, the tumor becomes visible when it is at least 0.7 cm in diameter.

Fig. 22 shows the quantitative version of our observations. We can see that the sensitivity is very low for a small size lesion, owing to the low number of photons emitted from it. The multihole collimator and the second wire-mesh collimator we

propose are in a good agreement in terms of sensitivity. The MSE of the images follows the same trend as in experiment A.

VII. Conclusion

In this paper, we demonstrated that the wire-mesh collimator design we propose is capable of replacing the multihole collimator, either used in conjunction with Wiener filtering image processing, where we reduce the weight of the original collimator by 60.5%, or without Wiener filtering, where the weight of the multihole collimator is reduced by 48.8%.

Even the first design we proposed, which was not acceptable as a replacement of the multihole collimator in terms of photon sensitivity, produced images of the phantom lesion that were of almost comparable quality as those produced by the multihole collimator, in terms of thresholds of minimum lesion activity and size for detectability.

We also showed that Wiener filtering, properly applied, can improve the images and increase the visibility of the tumor.

The apparent better performance of the second wire-mesh collimator we propose than that of the multihole collimator may be attributed to the random processes involved in the gamma camera.

Acknowledgment

The authors would like to thank Dr. M. Guy from the Royal Surrey County Hospital, Guildford, U.K., for providing the experimental data from the hospital, and Prof. N. Spyrou, A. Ma, and M. Alnafea from the Physics Department, University of Surrey, for their help with the MCNP code.

References

[1] H. O. Anger, "Scintillation camera with multichannel collimators," *J. Nucl. Med.*, vol. 5, pp. 515–531, 1964.

[2] K. Assie, V. Breton, I. Buvat, C. Comtat, S. Jan, M. Krieguer, D. Lazaro, C. Morel, M. Rey, G. Santin, L. Simon, S. Staelens, D. Strul, J. Vieira, and R. Van de Walle, "Monte Carlo simulation in PET and SPECT instrumentation using GATE," *Nucl. Instrum. Meth. Phys. Res. A*, vol. 527, no. 1–2, pp. 180–189, 2004.

[3] R. J. D. Beattie and J. Byrne, "A Monte Carlo program for evaluating the response of a scintillation counter to monoenergetic gamma rays," *Nucl. Instrum. Meth.*, vol. 104, pp. 163–168, 1972.

[4] J. Berthot, V. Breton, P. Brette, S. Crespin, N. Giokaris, D. Lazaro, J. Maublant, and L. Meritet, "Monte Carlo simulation of gamma-cameras using GEANT," in *Proc. IEEE Nuclear Science Symp. Conf. Rec.*, 2000, vol. 3, pp. 20/110–20/113.

[5] D. Boulfelfel, R. M. Rangayyan, L. J. Hahn, and R. Kloiber, "Three-dimensional restoration of single photon emission computed tomography images," *IEEE Trans. Nucl. Sci.*, vol. 41, no. 5, pp. 1746–1754, Sep. 1994.

[6] J. F. Briesmeister, *MCNP Data Manual*. Oak Ridge, TN: Radiation Safety Information Computational Center, 2001.

[7] A. C. Chamberlain, "Determination of an optimum wire mesh collimator and digital filter using Monte Carlo simulation," Ph.D. dissertation, Dep. Med. Phys., Medical Univ. Southern Africa, Pretoria, South Africa, Nov. 2001.

[8] D. J. de Vries, S. C. Moore, R. E. Zimmerman, S. P. Mueller, B. Friedland, and R. C. Lanza, "Development and validation of a Monte Carlo simulation of photon transport in an Anger camera," *IEEE Trans. Med. Imag.*, vol. 9, no. 4, pp. 430–438, Dec. 1990.

[9] D. D. Demers and R. A. Stein, "A modified Wiener filter for restoration of gated nuclear cardiac images," in *Proc. Annu. Int. Conf. IEEE Engineering in Medicine and Biology Society*, 1990, vol. 12, no. 1, pp. 156–157.

[10] D. D. Demers and R. A. Stein, "A parallel monte carlo code for planar and SPECT imaging: Implementation, verification and applications in ^{131}I SPECT," *Comput. Meth. Progr. Biomed.*, vol. 67, p. 115124, 2002.

[11] D. J. Dowsett, P. A. Kenny, and R. E. Johnston, *The Physics of Diagnostic Imaging*. New York: Chapman & Hall Medical, 1998.

[12] J. W. Goodman and J. F. Belsher, "Fundamental limitations in linear invariant restoration of atmospherically degraded images," *Proc. SPIE*, vol. 75, pp. 141–154, 1976.

[13] G. J. Gruber, "Monte Carlo simulations of breast tumor imaging properties with compact, discrete gamma cameras," *IEEE Trans. Nucl. Sci.*, vol. 46, no. 6, pp. 2119–2123, Nov. 1999.

[14] E. L. Hall, *Computer Image Processing and Recognition*. New York: Academic, 1979.

[15] N. Honda, K. Machida, J. Tsukada, H. Kaizu, and M. Hosoba, "Optimal preprocessing Butterworth-Wiener filter for Tl-201 rnyocardial SPECT," *Eur. J. Nucl. Med.*, vol. 13, pp. 404–407, 1987.

[16] P. Sprawls, Jr., *Physical Principles of Medical Imaging*. Gaithersburg, MD: Aspen, 1993.

[17] G. F. Knoll, *Radiation Detection and Measurement*, 2nd ed. New York: Wiley, 1989.

[18] M. Ljungberg, S.-E. Strand, and M. A. King, *Monte Carlo Calculations in Nuclear Medicine: Applications in Diagnostic Imaging*. Bristol, U.K.: Inst. Bristol Publishing, 1998.

[19] D. P. McElroy, E. J. Hoffman, L. MacDonald, B. E. Patt, J. S. Iwanczyk, Y. Yamaguchi, and C. S. Levin, "Evaluation of performance of dedicated, compact scintillation cameras," *IEEE Trans. Nucl. Sci.*, vol. 49, no. 3, pp. 794–801, May 2001.

[20] T. R. Miller and E. S. Rollins, "A practical method of image enhancement by interactive digital filtering," *J. Nucl. Med.*, vol. 26, no. 9, pp. 1075–1080, 1985.

[21] M. E. Nikalaou, G. Spyrou, G. Panayiotakis, and G. Tzanakos, "Design studies of collimated gamma ray sources," in *Proc. IEEE Nuclear Science Symp. Conf. Rec.*, 2000, vol. 3, pp. 20/100–20/104.

[22] K. Ogawa and J. Kato, "Collimator design for single photon emitter," in *Proc. IEEE Nuclear Science Symp. Conf. Rec.*, 2002, vol. 2, pp. 760–763.

[23] K. Ogawa and J. Kato, "Wired collimator for single photon emitter," *IEEE Trans. Nucl. Sci.*, vol. 50, no. 5, pp. 1536–1540, May 2003.

[24] M. Petrou and P. Bosdogianni, *Image Processing The Fundamentals*. New York: Wiley, 2000.

[25] W. H. Press, S. A. Teukolsky, W. T. Vetterling, and B. P. Flannery, *Numerical Recipes in C: The Art of Scientific Computing*. Cambridge, U.K.: Cambridge Univ. Press, 1992.

[26] J. D. Sain and H. H. Barrett, "Performance evaluation of a modular gamma camera using a detectibility index," *J. Nucl. Med.*, vol. 44, no. 1, pp. 58–65, 2003.

[27] S. Suthaharan and Z. Zhang, "SNR optimization using genetic algorithm," in *Proc. IEEE Int. Conf. Image Processing*, 1997, vol. 1, pp. 295–297.

[28] S. Webb, *The Physics of Medical Imaging*. Bristol, U.K.: Adam Hilger, 1988.

[29] N. Wiener, *Extrapolation, Interpolation, and Smoothing of Stationary Time Series: With Engineering Applications*. New York: Wiley, 1949.

[30] H. Zaidi, "Relevance of accurate Monte Carlo modeling in nuclear medical imaging," *Amer. Assoc. Phys. Med.*, vol. 26, no. 4, pp. 574–608, 1999.

M.-Iqbal Saripan (M'06) received the B.Eng. degree in electronic engineering from the Universiti Teknologi Malaysia in 2001 and the Ph.D. degree in image processing from the University of Surrey, Guildford, U.K., in 2006.

Currently, he is a Lecturer and coordinator for the Embedded and Intelligent System Engineering Research Group, Department of Computer and Communication Systems Engineering, Faculty of Engineering, Universiti Putra Malaysia. His research interests are in the area of medical imaging, speech processing, and embedded system.

Dr. Saripan is a member of the IEEE Engineering in Medicine and Biology Society.